Comparison of large-volume imaging approaches using computed tomography

Mattia Humbel[a], Christine Tanner[a,b], Griffin Rodgers[a], Hans Deyhle[a], Georg Schulz[a,b], and Bert Müller[a]

[a]Biomaterials Science Center, Department of Biomedical Engineering, University of Basel, Hegenheimermattweg 167B/C, 4123 Allschwil, Switzerland
[b]Core Facility Micro- and Nanotomography (MiNa), Department of Biomedical Engineering, University of Basel, Hegenheimermattweg 167B/C, 4123 Allschwil, Switzerland

ABSTRACT

The acquisition of large tomography volumes, exceeding the typical detector field-of-view, requires advanced acquisition techniques. Current approaches are the tiling of local reconstructed volumes or the tiling in projection space, also known as mosaic tomography. Reconstruction tiling has the advantage that standard reconstruction software can be used and acquisition can be interrupted and resumed relatively easily. The disadvantage is that there is the need for volume registration and transformation. Projection tiling is faster and more dose efficient, however a custom reconstruction pipeline is required, registration in projection space is challenging due to lower contrast, and there is a high sensitivity to mechanical instabilities. In this work we propose a third, hybrid approach, to profit from the advantages of projection tiling, but limit the risks. The volume to be imaged is covered by overlapping cylinders, each corresponding to the reconstructed volume of one mosaic tomogram. The number of rings per cylinder and the total number of cylinders can be tuned to the specimen at hand. We demonstrate this approach for a 2 cm-wide section of a human brain stem, imaged at the ANATOMIX beamline of Synchrotron SOLEIL, France with 0.65 µm voxel size, resulting in reconstructed slices 29,650 voxels wide. For mosaic reconstruction we used our team's existing pipeline. For stitching of volumes, image registration was performed in the overlap regions. As pairwise displacements between cylinders are not independent, we modified the registration approach to force a consistent solution. The results of the hybrid acquisition in seven tiles with four rings were compared to a pure projection tiling approach with eight rings and to local regions representing reconstruction tiling. In conclusion, we propose an extended field of view acquisition scheme building on the speed and dose efficiency of mosaic acquisition, but relaxing the requirements for mechanical and beam stability.

Keywords: Mosaic microtomography, hybrid tiling, extended field-of-view, brain stem, image registration

1. INTRODUCTION

The human brain has an average volume of 1130 cm^3 for women and 1260 cm^3 for men,[1] while the cell bodies of neurons range from 5 to 100 µm in diameter.[2] Thus, to image the entire brain with cellular resolution, one must cover length scales spanning five orders of magnitude. On the other hand, the detectors used for X-ray imaging typically have a field-of-view (FOV) limited to a few mm^2 for an effective pixel size around 1 µm. Therefore to image specimens that are several centimeters in diameter, the FOV needs to be extended. Conventionally there are two approaches for extending the FOV, either by stitching reconstructed volumes, or by stitching partial projections.[3] The schemes are illustrated in Fig. 1. Reconstruction tiling is relatively widely used and there exists software like BigStitcher (originally developed for light sheet microscopy)[4] or NRStitcher.[5] This has for example been used to image casts of the mouse brain vascular system,[6] or a rat lung.[7] Several approches have been used for optimizing the stitching positions. Preibisch *et al.* used pairwise registration of volumes by maximizing Fourier transform-based phase correlation and found optimal global transformations by solving a least-squares problem

Further author information: (Send correspondence to M.H.)
M.H.: E-mail: mattia.humbel@unibas.ch, Telephone: +41 (0)61 207 54 42
B.M.: E-mail: bert.mueller@unibas.ch, Telephone: +41 (0)61 207 54 30

Developments in X-Ray Tomography XV, edited by Bert Müller, Ge Wang,
Proc. of SPIE Vol. 13152, 1315211 · © 2024 SPIE
0277-786X · doi: 10.1117/12.3028566

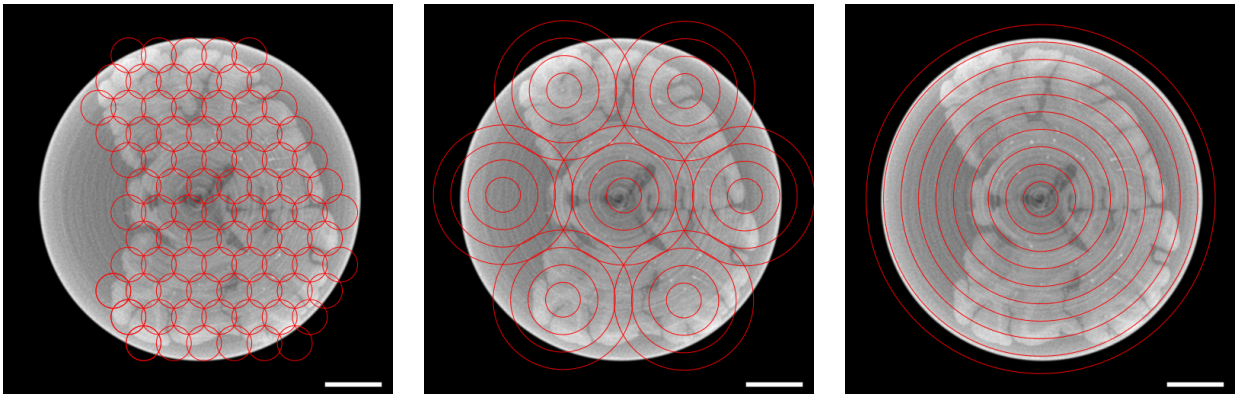

Figure 1. Illustration of tiling schemes for extended field-of-view imaging of a human brain sample. The images were acquired in the Phoenix Nanotom m. The red lines delineate the information provided by single scans. Left: Reconstruction tiling consists of the stitching of many individual local tomograms. Center: A hybrid tiling approach combines the ideas of projection and reconstruction tiling. Right: Projection tiling is implemented by acquiring radiographs at a series of rotation axis offset positions, in order to produce extended projections covering the entire specimen. Scale bars are 2 cm.

given these pairwise translations.[8] Bria and Iannello made use of a minimum spanning tree to optimize tile placements, which additionally takes into account the degree of reliability assigned to pairwise displacements.[9] The projection stitching approach has been in use for two decades in form of tomographic acquisition with an asymmetric rotation axis position and 360° rotation. Müller *et al.* have employed it for the study of middle and inner ear implants.[10] This approach has been extended to stitching more than two partial projections acquired at a series of laterally offset rotation axis positions. Vescovi *et al.* have used phase correlation on pairs of radiographs for projection stitching,[11] and have implemented this in the *Tomosaic* framework.[12] Instead of correlating projections, it is also possible to perform the correlation and stitching on sinograms, as demonstrated by Vo *et al.*[13] Under the right conditions, both the reconstruction tiling and projection tiling approaches have been observed to provide reasonable image quality.[14] For reconstruction tiling, the artefacts due to truncated sinograms are a prominent concern. These depend on the degree of truncation, as well as the geometry and composition of the imaged object, so the suitability needs to be assessed for each case. Projection tiling does not suffer from this, however it is sensitive towards a tilting of the rotation axis and to accumulation of registration error.[15] Overall projection tiling is more time and dose efficient for approximately cylindrical specimens.[16] We propose a hybrid approach, combining both projection and reconstruction tiling, balancing the time and dose efficiency of the former and the resilience of the latter. This approach is tested on a specimen of brain tissue with 2 cm diameter and compared to equivalent scans with projection and reconstruction tiling, respectively.

2. MATERIALS AND METHODS

A human cerebellum was extracted *post mortem* and fixated in paraformaldehyde. A cylindrical section 2 cm in diameter was prepared and immersed in 100 % ethanol for X-ray imaging. The study was authorized by the ethics commission of northwestern and central Switzerland (EKNZ) under project number 2020-00047.

Microtomography measurements were performed at the ANATOMIX beamline of Synchrotron SOLEIL, France.[17] The undulator gap was set to 5.7 mm. 20 µm gold and 100 µm copper were inserted into the beam path to attain a filtered white beam with a mean photon energy around 38 keV. The specimen was placed 50 mm away from the detector setup to utilize propagation-based phase contrast. A 10× magnifying lens optic and a Hamamatsu Orca Flash 4.0 V2 CMOS camera were used to obtain an effective pixel size of (0.6504 ± 0.0004) µm. The exposure time per image was set to 100 ms.

For ring acquisition, the rotation axis was offset from its center position in steps of 1.2 mm, starting at 0.6 mm offset for the innermost ring. For the eight concentric rings covering the whole specimen cross section, 18,000 projections were acquired over 360° for each ring. The partial projections were stitched based on image correla-

tion, as described in a previous publication,[3] resulting in sinograms 29,650 pixels wide and then reconstructed using *TomoPy*.[18]

For the hybrid approach, the specimen cross section area was covered with seven tiles arranged in a hexagonal geometry, similar to Fig. 1, each consisting of four concentric rings. To acquire one tile, the specimen position on top of the rotation axis was adjusted accordingly, before then proceeding with the ring acquisition scheme described above. The 9000 projections were acquired over 360° for each of the four rings. The resulting stitched projections were 14,000 pixels wide. Each tile was reconstructed by the pipeline established for projection stitching. For alignment of the resulting cylindrical tiles, cuboid regions in the overlap between tiles were identified, and pairwise registration with a translation transform model and normalized correlation coefficient as image similarity measure was performed using *Elastix*.[19,20] Globally optimal translation parameters for the tiles were computed using least squares optimization based on the results of pairwise registration, as described by Preibisch *et al.*[8] The slices were transformed to a common volume and linear blending was applied in the overlaps.

To demonstrate the volume tiling approach, five half-acquisition scans located from the specimen's center to its border along a straight line were acquired. We collected 18,000 projections, same as for the ring acquisition.

In order to compare the suitability of the presented extended field-of-view acquisition approaches for imaging the entire human brain, which is around 12 cm in diameter, *i.e.* six times larger than the 2 cm wide specimen examined here, the time requirements for imaging and reconstruction were estimated. For estimating the reconstruction time, a series of test reconstructions were performed and the time recorded. For all test measurements the ratio of the number of projections to the width of the sinograms was set to 0.6. The reconstructions were performed using the `gridrec`-Algorithm[21,22] in TomoPy.[18] The computations were performed on an HP Z640 Workstation. For the elapsed time the average of 10 runs was measured. For the acquisition setup, the KIT CMOS camera in operation at the P07 beamline at PETRA III, DESY, Hamburg, Germany was considered with 5120×3840 pixel FOV. An effective voxel size of 1.2 µm and acquisition time of 30 ms was assumed. To account for the sample geometry, the outlines of the brain slice shown in Fig. 1 were considered, and the number of tiles was tuned to cover this area. A range of hybrid tiling approaches were considered, with the number of lateral FOV extensions, or *rings*, per tile taking values between 1 and 10. For each case, the number of tiles necessary to cover the specimen cross-section area was determined. Acquiring one ring per tile corresponds to reconstruction stitching, while ten rings are sufficient to cover the specimen with one tile, which corresponds to the projection stitching scheme. For estimating the acquisition time, the number of projections was assumed to be 0.6 times the width of the respective stitched sinogram, consistent with the configuration used in the reconstruction time measurements.

3. RESULTS

The projection tiling approach with acquisition of eight concentric rings required a total scan time of four hours. The volume covered was a cylinder 13 mm high and 193 mm in diameter. A virtual slice is shown in Fig. 2. In the cerebellum we can discern granule cells, Purkinje cells, the molecular layer and the vasculature. The reconstructed volume from blended and phase-retrieved projections shows a fairly homogeneous distribution of gray values, with a slight background gradient visible with lower intensities towards the center of the reconstructed volume, likely due to beam hardening.

For the combined reconstruction and projection tiling approach (hybrid acquisition) we observed a similar level of details visible in the reconstructed volume. Fig. 3 shows this for a region of interest in the cerebellum, where the granular layer with individual granule cells, the molecular layer and a blood vessel are discernible. The matching of intensity levels between the reconstructed tiles proved challenging. The overlapping parts of neighboring tiles were used to shift the mean intensity of the outer tiles to match that of the central tile. However, due to the background gradients introduced by local tomography resulting in higher intensities towards the peripheral parts of each tile, this approach proved not adequate to achieve the expected homogeneous distribution of intensities. Therefore in the combined volume shown in Fig. 3 the borders between tiles remain visible and the material in the central tile appears brighter, although it is the same tissue.

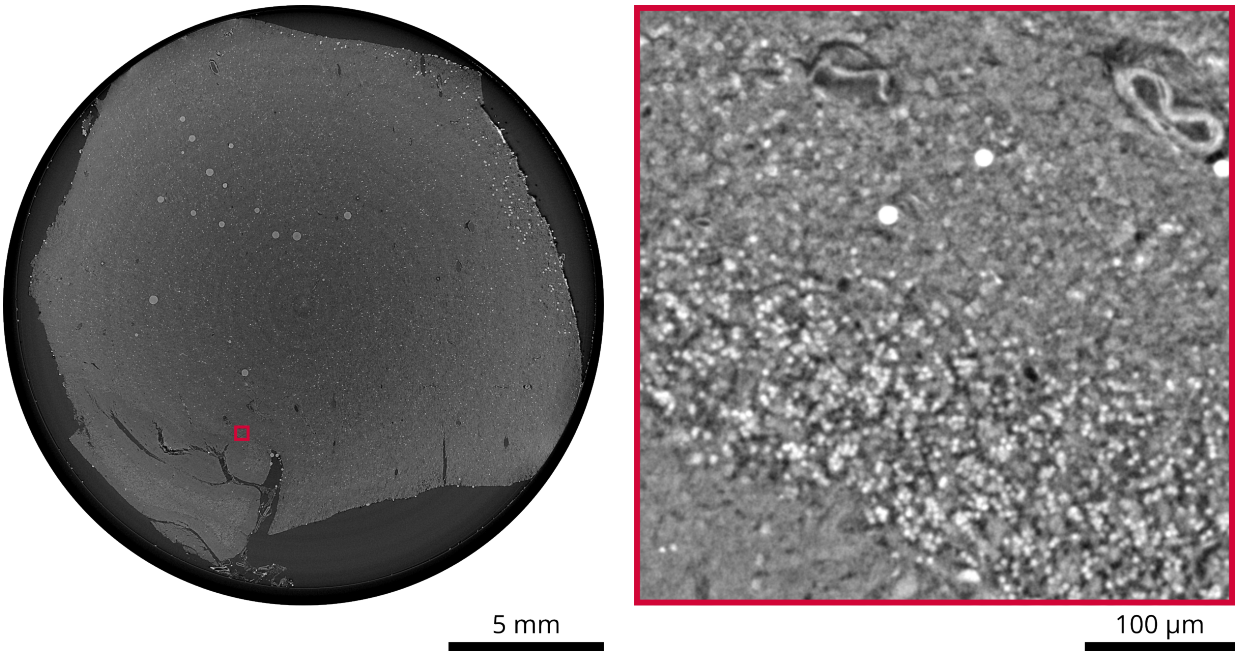

Figure 2. Results of the projection tiling acquisition. Left: Virtual slice through the acquired volume. Right: Enlarged region of interest located in the cerebellum.

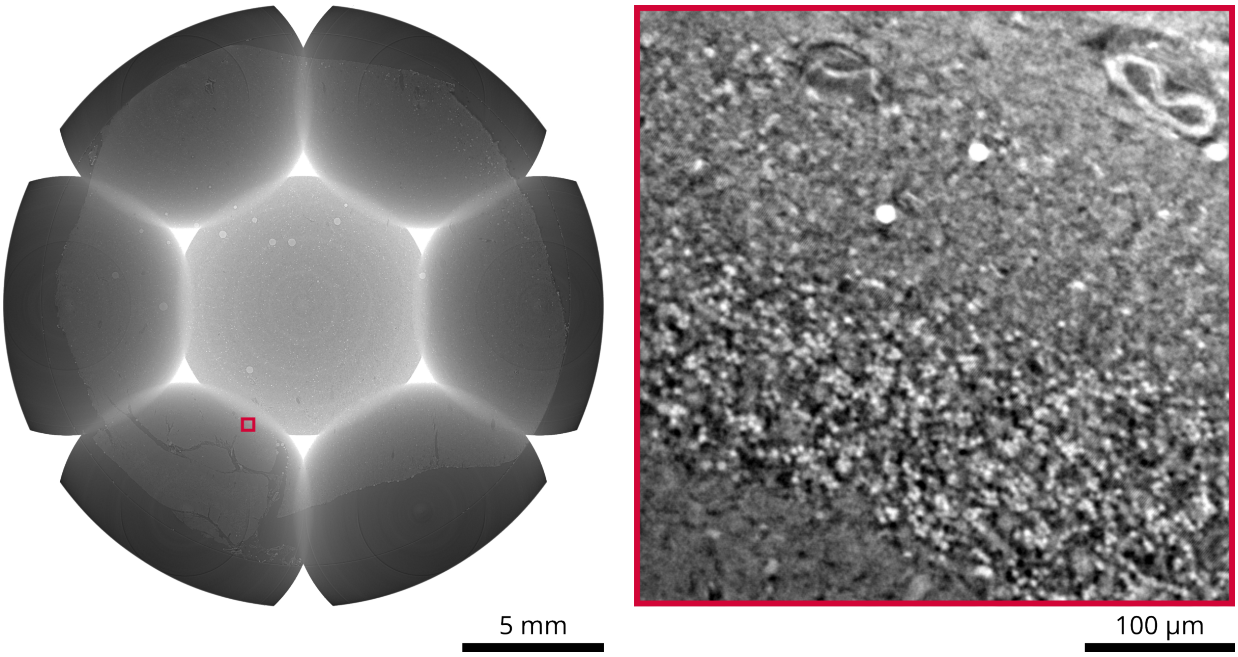

Figure 3. Results of the hybrid tiling acquisition. Left: Virtual slice through the acquired volume. The intensities in the outer regions were rescaled such that the mean intensities in the overlaps with the central tile were in agreement. Due to the present cupping artefacts, there is still some disagreement in the intensity levels. Right: Same region of interest as in Fig. 2.

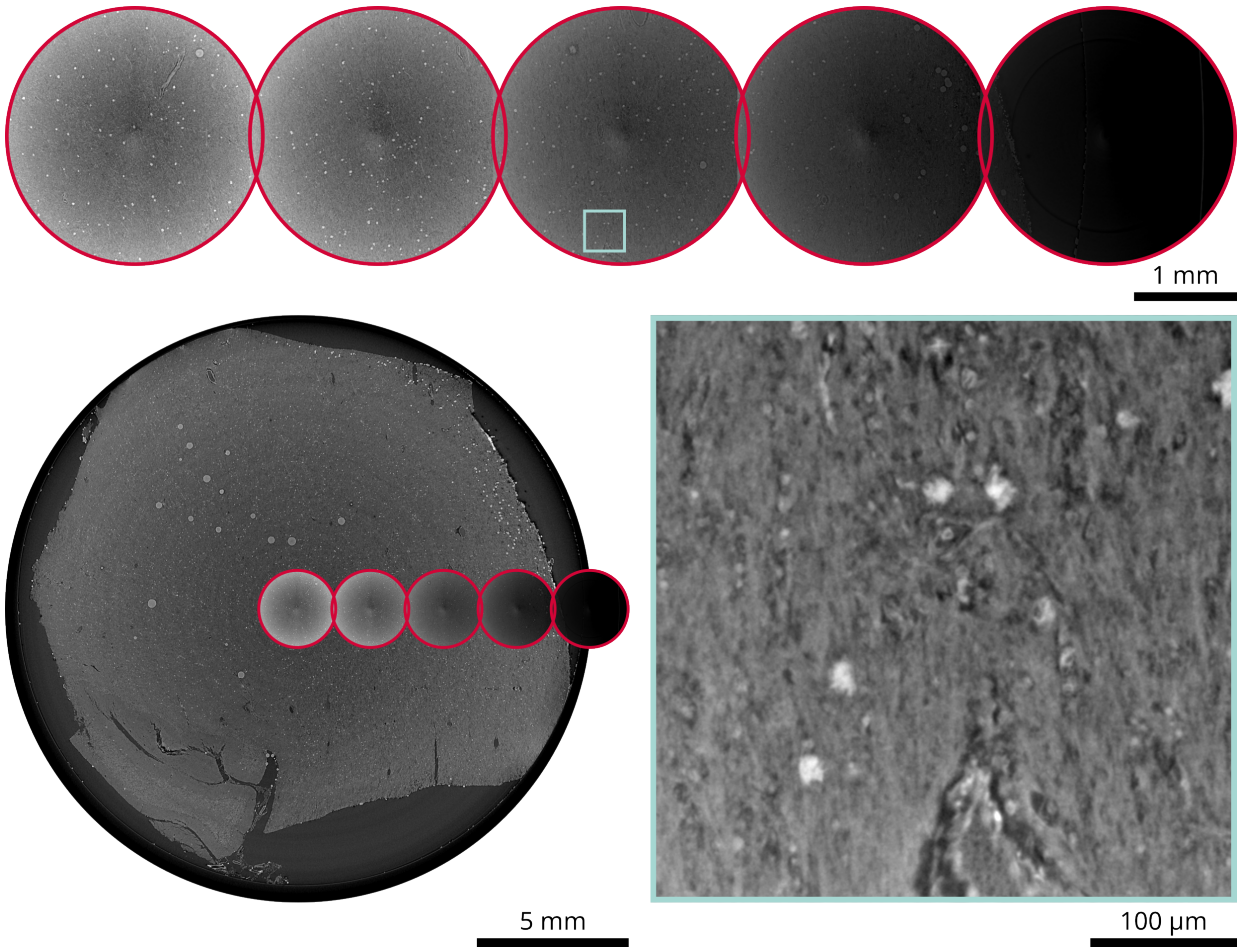

Figure 4. Results of the stitching of local tomograms. Top: Virtual slice through the acquired volume. Bottom left: Location of the five tiles with respect to the total sample volume. Bottom right: Enlarged region of interest.

The reconstruction tiling approach was demonstrated by five local tomograms arranged radially from the center of the specimen to its border that were stitched after reconstruction. As shown in Fig. 4, there is a considerable gradient in the measured image intensities due to the high degree of locality in these acquisitions. Each local tomogram was reconstructed from 18,000 projections, which is the same number as for the eight ring projection stitching scan. Thus, although the number of projections for the local tomograms was chosen adequate to the whole specimen diameter, as suggested for example by Kyrieleis *et al.*,[23] the overall gradient is still present. While for the central tile the amount of material outside the field-of-view is approximately equal in all azimuthal directions, for the outer tiles this distribution is highly anisotropic. Judging from visual inspection of anatomical features, the spatial resolution offered by this approach is similar to the other two.

Weighing the schemes for extended field-of-view acquisition against each other must include considering the trade-off between acquisition time and processing time. These were estimated for the case of one virtual slice through a human brain to be measured using a 5120 pixel detector FOV at 30 ms exposure time per frame and 1.2 µm voxel size. The number of projections was assumed to depend on the width of the stitched sinogram by a constant factor, here chosen as 0.6. As a basis for the estimation of the reconstruction time, trial reconstructions were performed on sinograms with width n ranging from 2000 to 32,768 pixels. As can be observed in Fig. 5, the reconstruction times are optimal for n a power of two and otherwise follow roughly a step function. The reason is that the implementation of the `gridrec` algorithm in TomoPy involves padding the data to a size equal to the next power of two along directions in which Fourier transforms are performed, as the fast Fourier

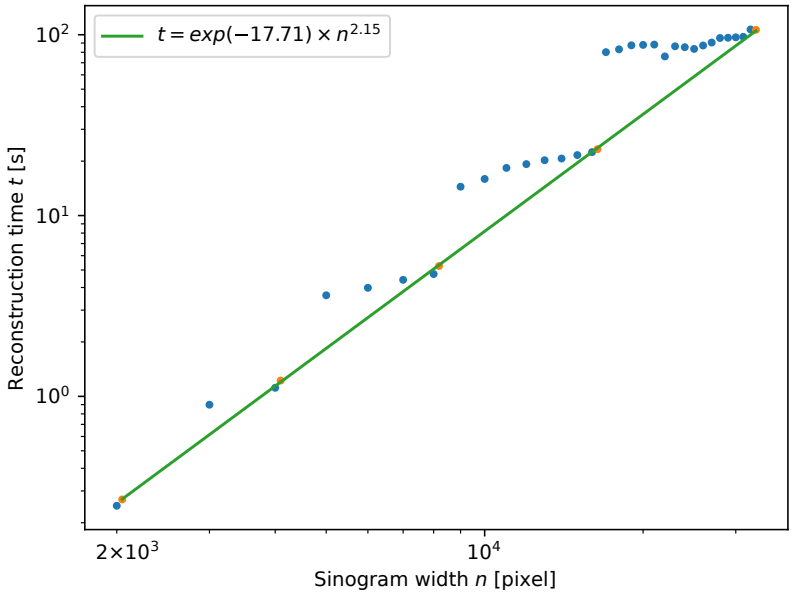

Figure 5. Time for reconstruction of one slice from a sinogram n pixels wide and with $0.6 \times n$ projections. The orange dots highlight the case where n is a power of two, *i.e.* 2^{11} to 2^{16}, and the green line illustrates the fit of a power function to approximate the performance for n a power of two.

transform is most efficient when the number of points is a power of two. For n a power of two, the time t is reasonably approximated by $t = e^{-17.71} \times n^{2.15}$. Thus, for the following calculations, the reconstruction time was estimated by rounding up n to the next power of two, and applying the formula above. Fig. 6 demonstrates the trade-off between acquisition and reconstruction time. It shows that certain configurations are clearly not suitable for the given geometry, specifically those with seven, eight, or nine rings per tile, as either there is a setup with the same number of tiles but less rings, or the tiles would be arranged with much overlap or large portions of air being measured. For tiles with eight or nine rings, the sinogram widths fall between the same two powers of two, therefore in our approximation the reconstruction times for both are equal. In practice the processing time for eight rings will be a bit faster, judging from the results of the test measurements in Fig. 5. Note that the reconstruction times were measured for the processing of a single slice on a consumer-grade CPU utilizing one core. The processing could likely be further optimized, however the relative time difference observed between acquisition schemes should remain valid. The `gridrec` algorithm on CPU was evaluated as the larger sinograms grow too large to be easily processed within the limits of GPU memory. Further note that a) only the reconstruction time is considered here, not the time required for stitching, and b) eventual padding of sinograms was not considered. The former affects all tiling approaches, and it depends on the details of the stitching process whether it would influence processing time in favor of one or the other. The latter means that we are likely underestimating the processing time for reconstruction tiling, as generally more padding is needed for sinograms with a higher degree of truncation. Finally, the number of projections was determined only from the size of the respective reconstructed region. However, it has been suggested that the size of the entire specimen should be considered even for local tomograms,[23] which would increase both acquisition and reconstruction time for reconstruction tiling and hybrid approaches.

4. DISCUSSION

The results presented here demonstrate the possibility of conducting a projection tiling measurement with 16 times laterally extended field-of-view without showing effects of a rotation axis misalignment. For this measurement at the Anatomix beamline at Synchrotron Soleil, no beam instability could be observed over the

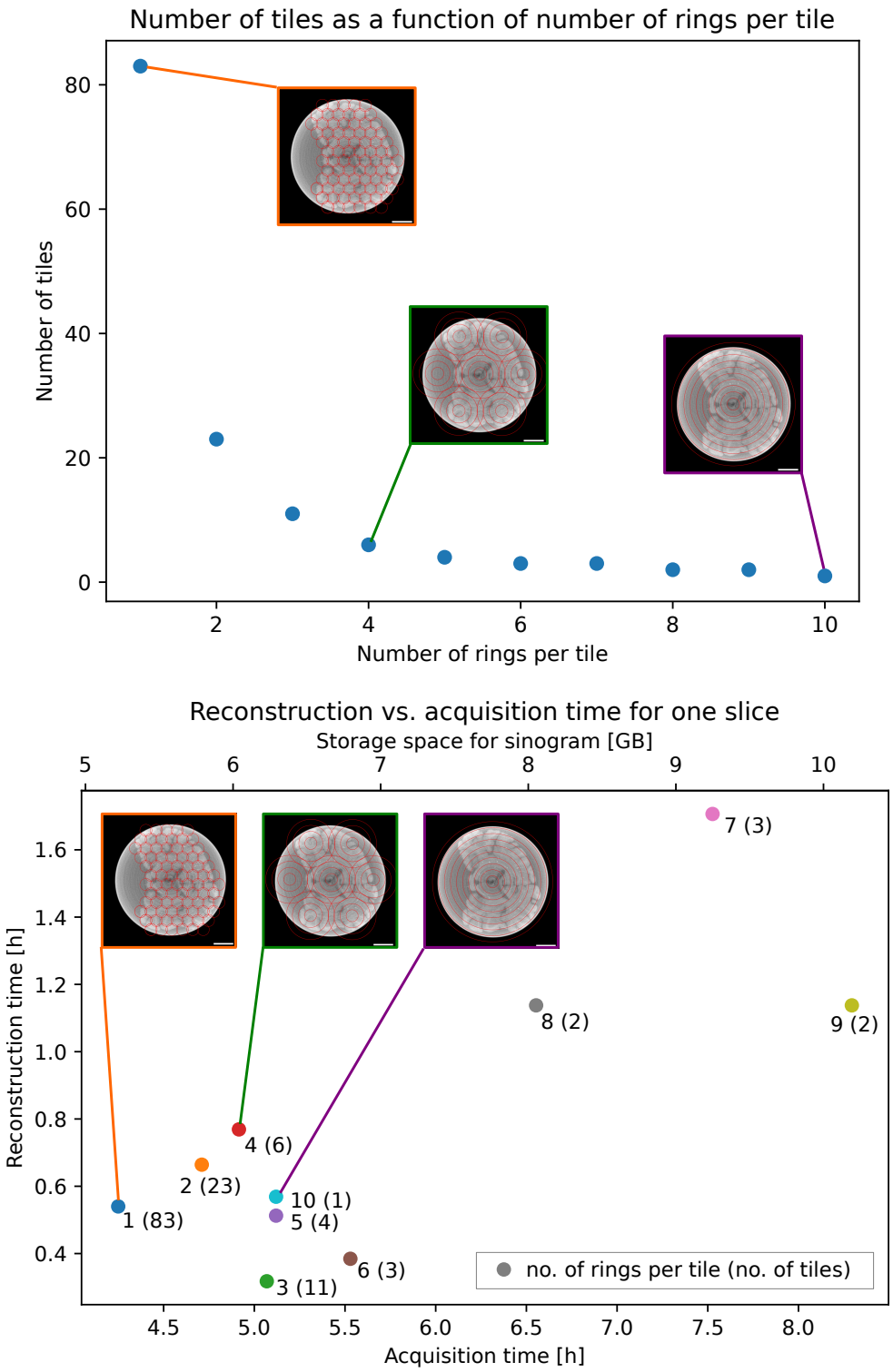

Figure 6. Estimations for the trade-off between acquisition time and processing time for projection tiling, reconstruction tiling, and hybrid acquisition strategies, considering an entire brain specimen. Top: Number of tiles required to cover the specimen in a hybrid tiling approach, given the number of rings constituting one tile. One ring per tile corresponds to pure reconstruction tiling, while a single tile with many rings corresponds to projection tiling. Bottom: Given the number of rings per tile, this shows an estimation of the time required for the acquisition and the time for reconstruction.

30 min scan time required to acquire one of the eight rings with 18,000 projections in flyscan mode. As an alternative, a hybrid acquisition approach with half the number of rings for projection tiling was demonstrated and compared to a pure reconstruction tiling scheme. Local tomography artefacts could be observed both for the hybrid and the reconstruction tiling approach. In the first case, these could likely be alleviated by sufficient padding of the sinograms.[23] In the second case, an intensity gradient could be observed not only within individual reconstructed volumes, but also spanning from central to peripheral tiles. Removing this would require an additional processing step. An estimate of acquisition and processing times for reconstruction and projection tiling, as well as a range of hybrid schemes in between, illustrated the trade-off explored by Fransson *et al.*[16] between the optimized acquisition time offered by pure projection tiling, and the efficient reconstruction possible for reconstruction tiling. Hybrid tiling was established as a viable option in between. The estimates presented in Fig. 6 were based on a very optimistic assumption about the angular sampling requirements for local tomography acquisitions independent of the degree of sinogram truncation. Were the number of projections adjusted for the extent of the entire specimen, the acquisition times would increase drastically for schemes with many small tiles. Therefore, the number of projections necessary for achieving reasonable image quality for highly local tomograms is of central importance when comparing acquisition times between tiling schemes. When treating biological specimen, radiation dose is an additional factor to be considered. While the total deposited dose in general scales linearly with acquisition time, its distribution over time and space is also relevant. This has been shown to be more favorable in projection tiling,[12] but the implications for hybrid acquisition schemes still need to be investigated.

5. CONCLUSION

For acquiring large volumes at high resolution, a projection stitching approach is highly suitable, as long as the mechanical stability of both the specimen and the measurement setup is given for acquisition times of several hours. Blending of data in the projection domain is quite straightforward compared to the reconstructed volume domain. The preferred tiling scheme with respect to acquisition time and dose efficiency depends on the angular sampling requirements for local tomography. If the number of projections is chosen independent of overall specimen width, reconstruction tiling is faster. If that is not permissible, projection tiling is the more time and dose efficient approach. For the cases where the mechanical stability requirements are not given, the hybrid approach we presented can be considered a viable compromise. It combines at heightened resilience towards sample deformation compared with projection tiling, and potentially decreased acquisition time and number of three-dimensional volumes to be transformed compared with reconstruction tiling. The current study has demonstrated that for a 2 cm wide brain sample and an effective voxel size of 0.65 µm, the mechanical stability requirements are fulfilled at a state-of-the-art microtomography beamline.

ACKNOWLEDGMENTS

The authors thank Timm Weitkamp of Synchrotron Soleil, France for his active support during the beamtime at Anatomix, and Magdalena Müller-Gerbl, University of Basel, Switzerland, for provision of the specimen.

Beamtime at the Anatomix beamline was granted by Synchrotron Soleil under proposal no. 20220597. Anatomix is an Equipment of Excellence (EQUIPEX) funded by the *Investments for the Future* program of the French National Research Agency (ANR), project *NanoimagesX*, grant no. ANR-11-EQPX-0031.

M.H. acknowledges financial support from the Swiss National Science Foundation grants no. 185058 and 213535.

REFERENCES

[1] Cosgrove, K. P., Mazure, C. M., and Staley, J. K., "Evolving Knowledge of Sex Differences in Brain Structure, Function, and Chemistry," *Biological Psychiatry* **62**, 847–855 (Oct. 2007).

[2] Pannese, E., "III. Shape and Size of Neurons," in [*Neurocytology: Fine Structure of Neurons, Nerve Processes, and Neuroglial Cells*], Pannese, E., ed., 13–23, Springer International Publishing, Cham (2015).

[3] Rodgers, G., Tanner, C., Schulz, G., Weitkamp, T., Scheel, M., Girona Alarcón, M., Kurtcuoglu, V., and Müller, B., "Mosaic microtomography of a full mouse brain with sub-micron pixel size," in [*Developments in X-Ray Tomography XIV*], **12242**, 353–365, SPIE (Oct. 2022).

[4] Hörl, D., Rojas Rusak, F., Preusser, F., Tillberg, P., Randel, N., Chhetri, R. K., Cardona, A., Keller, P. J., Harz, H., Leonhardt, H., Treier, M., and Preibisch, S., "BigStitcher: Reconstructing high-resolution image datasets of cleared and expanded samples," *Nature Methods* **16**, 870–874 (Sept. 2019).

[5] Miettinen, A., Oikonomidis, I. V., Bonnin, A., and Stampanoni, M., "NRStitcher: Non-rigid stitching of terapixel-scale volumetric images," *Bioinformatics* **35**, 5290–5297 (Dec. 2019).

[6] Wälchli, T., Bisschop, J., Miettinen, A., Ulmann-Schuler, A., Hintermüller, C., Meyer, E. P., Krucker, T., Wälchli, R., Monnier, P. P., Carmeliet, P., Vogel, J., and Stampanoni, M., "Hierarchical imaging and computational analysis of three-dimensional vascular network architecture in the entire postnatal and adult mouse brain," *Nature Protocols* **16**, 4564–4610 (Oct. 2021).

[7] Borisova, E., Lovric, G., Miettinen, A., Fardin, L., Bayat, S., Larsson, A., Stampanoni, M., Schittny, J. C., and Schlepütz, C. M., "Micrometer-resolution X-ray tomographic full-volume reconstruction of an intact post-mortem juvenile rat lung," *Histochemistry and Cell Biology* **155**, 215–226 (Feb. 2021).

[8] Preibisch, S., Saalfeld, S., and Tomancak, P., "Globally optimal stitching of tiled 3D microscopic image acquisitions," *Bioinformatics* **25**, 1463–1465 (June 2009).

[9] Bria, A. and Iannello, G., "TeraStitcher - A tool for fast automatic 3D-stitching of teravoxel-sized microscopy images," *BMC Bioinformatics* **13**, 316 (Nov. 2012).

[10] Müller, B., Bernhardt, R., Weitkamp, T., Beckmann, F., Bräuer, R., Schurigt, U., Schrott-Fischer, A., Glueckert, R., Ney, M., Beleites, T., Jolly, C., and Scharnweber, D., "Morphology of bony tissues and implants uncovered by high-resolution tomographic imaging," *International Journal of Materials Research* **98**, 613–621 (July 2007).

[11] Vescovi, R. F. C., Cardoso, M. B., and Miqueles, E. X., "Radiography registration for mosaic tomography," *Journal of Synchrotron Radiation* **24**, 686–694 (May 2017).

[12] Vescovi, R., Du, M., de Andrade, V., Scullin, W., Gürsoy, D., and Jacobsen, C., "Tomosaic: Efficient acquisition and reconstruction of teravoxel tomography data using limited-size synchrotron X-ray beams," *Journal of Synchrotron Radiation* **25**, 1478–1489 (Sept. 2018).

[13] Vo, N. T., Atwood, R. C., Drakopoulos, M., and Connolley, T., "Data processing methods and data acquisition for samples larger than the field of view in parallel-beam tomography," *Optics Express* **29**, 17849–17874 (June 2021).

[14] Kyrieleis, A., Ibison, M., Titarenko, V., and Withers, P. J., "Image stitching strategies for tomographic imaging of large objects at high resolution at synchrotron sources," *Nuclear Instruments and Methods in Physics Research Section A: Accelerators, Spectrometers, Detectors and Associated Equipment* **607**, 677–684 (Aug. 2009).

[15] Du, M., Di, Z., Gürsoy, D., Xian, R. P., Kozorovitskiy, Y., and Jacobsen, C., "Upscaling X-ray nanoimaging to macroscopic specimens," *Journal of Applied Crystallography* **54**, 386–401 (Apr. 2021).

[16] Fransson, M., Cordonnier, B., Zimmermanns, R., Shearing, P. R., Rack, A., and Broche, L., "A comparison of stitching techniques to reconstruct large volume x-ray tomography of batteries," *Tomography of Materials and Structures* **5**, 100029 (June 2024).

[17] Weitkamp, T., Scheel, M., Giorgetta, J. L., Joyet, V., Roux, V. L., Cauchon, G., Moreno, T., Polack, F., Thompson, A., and Samama, J. P., "The tomography beamline ANATOMIX at Synchrotron SOLEIL," *Journal of Physics: Conference Series* **849**, 012037 (June 2017).

[18] Gürsoy, D., De Carlo, F., Xiao, X., and Jacobsen, C., "TomoPy: A framework for the analysis of synchrotron tomographic data," *Journal of Synchrotron Radiation* **21**, 1188–1193 (Sept. 2014).

[19] Klein, S., Staring, M., Murphy, K., Viergever, M. A., and Pluim, J. P. W., "Elastix: A Toolbox for Intensity-Based Medical Image Registration," *IEEE Transactions on Medical Imaging* **29**, 196–205 (Jan. 2010).

[20] Shamonin, D. P., Bron, E. E., Lelieveldt, B. P., Smits, M., Klein, S., and Staring, M., "Fast Parallel Image Registration on CPU and GPU for Diagnostic Classification of Alzheimer's Disease," *Frontiers in Neuroinformatics* **7** (Jan. 2014).

[21] Dowd, B. A., Campbell, G. H., Marr, R. B., Nagarkar, V. V., Tipnis, S. V., Axe, L., and Siddons, D. P., "Developments in synchrotron x-ray computed microtomography at the National Synchrotron Light Source," in [*Developments in X-Ray Tomography II*], **3772**, 224–236, SPIE (Sept. 1999).

[22] Rivers, M. L., "tomoRecon: High-speed tomography reconstruction on workstations using multi-threading," in [*Developments in X-Ray Tomography VIII*], **8506**, 169–181, SPIE (Oct. 2012).

[23] Kyrieleis, A., Titarenko, V., Ibison, M., Connolley, T., and Withers, P., "Region-of-interest tomography using filtered backprojection: Assessing the practical limits," *Journal of Microscopy* **241**(1), 69–82 (2011).